First oxidation products from the reaction of hydroxyl radicals with isoprene for pristine environmental conditions

Berndt, Torsten

2019-02-21

Berndt , T , Hyttinen , N , Herrmann , H & Hansel , A 2019 , ' First oxidation products from the reaction of hydroxyl radicals with isoprene for pristine environmental conditions ' , Communications chemistry , vol. 2 , 21 . https://doi.org/10.1038/s42004-019-0120-9

http://hdl.handle.net/10138/306005
https://doi.org/10.1038/s42004-019-0120-9

COMMUNICATIONS CHEMISTRY

ARTICLE

https://doi.org/10.1038/s42004-019-0120-9 OPEN

First oxidation products from the reaction of hydroxyl radicals with isoprene for pristine environmental conditions

Torsten Berndt [1], Noora Hyttinen[2], Hartmut Herrmann [1] & Armin Hansel [3]

Isoprene, C_5H_8, inserts about half of the non-methane carbon flux of biogenic origin into the atmosphere. Its degradation is primarily initiated by the reaction with hydroxyl radicals. Here we show experimentally the formation of reactive intermediates and corresponding closed-shell products from the reaction of hydroxyl radicals with isoprene for low nitric oxide and low hydroperoxy radical conditions. Detailed product analysis is achieved by mass spectrometric techniques. Quantum chemical calculations support the usefulness of applied ionization schemes. Observed peroxy radicals are the isomeric HO-$C_5H_8O_2$ radicals and their isomerization products HO-$C_5H_8(O_2)O_2$, bearing most likely an additional hydroperoxy group, and in traces HO-$C_5H_8(O_2)_2O_2$ with two hydroperoxy groups. Main closed-shell products from unimolecular peroxy radical reactions are hydroperoxy aldehydes, $C_5H_8O_3$, and smaller yield products with the composition $C_5H_8O_4$ and $C_4H_8O_5$. Detected signals of $C_{10}H_{18}O_4$, $C_{10}H_{18}O_6$, and $C_5H_{10}O_2$ stand for products arising from peroxy radical self- and cross-reactions.

[1] Atmospheric Chemistry Department (ACD), Leibniz-Institute for Tropospheric Research, TROPOS, 04318 Leipzig, Germany. [2] Department of Chemistry and Institute for Atmospheric and Earth System Research (INAR), University of Helsinki, 00014 Helsinki, Finland. [3] Institute for Ion Physics and Applied Physics, University of Innsbruck, 6020 Innsbruck, Austria. Correspondence and requests for materials should be addressed to T.B. (email: berndt@tropos.de)

Hydrocarbons with biogenic origin account for about 90% of the total volatile organic compounds emitted into Earth's atmosphere[1]. Isoprene represents the most abundant non-methane hydrocarbon in this process with an estimated emission rate of about 600×10^6 metric tons of carbon per year[2]. The emission rate may be altered in the future due to changes of environmental conditions[3].

Isoprene's degradation process is initiated by the reaction with atmospheric oxidants where the reaction with OH radicals is distinctly dominant[4]. The subsequent oxidation pathways and formed products influence the tropospheric chemistry, especially in isoprene-dominated areas such as in the tropics or other large forestlands[5–7]. A mechanistic understanding of the OH + isoprene reaction in the atmosphere has already been the subject of a large number of investigations up to now and the progress is tightly connected to the development of analytical techniques and the improvement of theoretical calculations[8].

OH attack of the conjugated diene system may occur at the four different diene carbon atoms with a preference of terminal OH addition forming allyl radicals[9]. Subsequently, reversible O_2 addition to the allyl system generates β- and δ-HO-$C_5H_8O_2$ radicals[10,11]. The reversibility of the O_2 addition makes an interconversion of the different RO_2 radical isomers possible. Available room-temperature rate coefficients of HO-$C_5H_8O_2$ radical decomposition to the corresponding allyl radicals and O_2 are in the range of 0.018–4 s^{-1}[12] or 0.14–16 s^{-1}[13], indicating that about 1 min[12] or 10 s[13] are needed to equilibrate the HO-$C_5H_8O_2$ radical distribution. Observations of HO-$C_5H_8O_2$ radicals have been previously reported using either UV absorption measurements for elevated RO_2 radical concentrations[14] or detection by mass spectrometry in a low-pressure experiment at 1–2 Torr He[15]. Figure 1 shows a scheme of the first reaction steps from OH attack at the 1-position, which is based on the current knowledge in the literature[11–13]. The products from this reaction are marked with "I". The formation of the analogous products starting from OH attack at the 4-position, marked with "II", is depicted in Supplementary Fig. 1. OH attack in 2- and 3-position accounts for ≤ 5% of the initial OH adduct distribution each and will not be further considered here[8,9,11,16]. Possible bimolecular RO_2 radical reactions with NO, HO_2, or other RO_2 radicals have been omitted to keep the schemes as lucid as possible, drawing the attention to the unimolecular RO_2 reactions. As a result of theoretical calculations, Peeters et al.[11] first suggested RO_2 isomerization steps that are competing with the well-established bimolecular RO_2 radical reactions in the atmosphere. According to that work, fast 1,6 H-shift of the *Z*-δ-HO-$C_5H_8O_2$ radicals forming hydroxy–hydroperoxy allyl radicals was predicted with rate coefficients higher than 1 s^{-1}[11], which were later revised to somewhat lower values[12]. Continuous reproduction of the *Z*-δ-HO-$C_5H_8O_2$ radicals from the whole RO_2 radical reservoir via RO_2 interconversion enables the 1,6 H-shift step to become an important exit channel in the case of less efficient bimolecular RO_2 reactions. The RO_2 radical resulting from O_2 addition at the α-position to the OH group of the hydroxy–hydroperoxy allyl radical, HO-$C_5H_8(O_2)O_2$_1 I in Fig. 1, rapidly decomposes forming an unsaturated hydroperoxy aldehyde, HPALD I, along with HO_2[11,17]. Experimental support for HPALD formation came from chamber experiments[13,18] and from a flow tube study[19].

O_2 addition at the γ-position relative to the OH group forms an RO_2 radical, HO-$C_5H_8(O_2)O_2$_2 I, which very rapidly undergoes an enolic 1,6 H-shift[20] generating an alkyl radical. The alkyl radical is believed to either add O_2 resulting in the next RO_2 radical, HO-$C_5H_8(O_2)_2O_2$ I, or to decompose forming an epoxy hydroperoxy carbonyl, $C_5H_8O_4$ I, along with an OH radical[12,13]. It should be noted that there is no proof for the epoxide structure of $C_5H_8O_4$ I proposed by Teng et al.[13]. Decomposition of the RO_2 radical, HO-$C_5H_8(O_2)_2O_2$ I, is expected to lead to a dihydroperoxy carbonyl, $C_4H_8O_5$ I, after H-shift reactions and subsequent elimination of CO and an OH radical[12]. Experimental evidence for the formation of a $C_4H_8O_5$ product is missing up to now. On the other hand, Teng et al.[13] observed a product signal by means of mass spectrometry being in line with the composition of $C_5H_8O_4$. It should be noted that 1,5 H-shift isomerization of the β-OH-$C_5H_8O_2$ radicals has been also discussed as a result of theoretical calculations[11,12,21]. The predicted rate, however, is relatively small, making 1,5 H-shift steps less important for the product formation of OH + isoprene.

Here we report on the direct probing of the initially formed RO_2 radicals and closed-shell products from the atmospheric reaction of OH radicals with isoprene conducted in a flow system[22,23]. With the exception of runs in the presence of NO, RO_2 radical consumption by bimolecular reactions were less important due to the kinetic limitation for a reaction time of 7.9 s or less and the low concentrations of RO_2 radicals and possible co-reactants. Hence, RO_2 isomerization steps and the resulting product formation were observable for conditions of less important bimolecular RO_2 radical reactions. The results provide experimental-based insight into the first reaction steps of the OH + isoprene reaction with special attention to RO_2 isomerization. This, together with other recent developments[12,13], allows a more exact description of isoprene's oxidation pathways in atmospheric modeling.

Results

Detected products from OH + isoprene. Efficient mass spectrometric detection of RO_2 radicals and closed-shell products is achieved by atmospheric pressure ionization using aminium, i.e., protonated *n*-propyl-, ethyl- or methylamine, or hydrazinium, i.e., protonated hydrazine, as the reagent ions. *n*-Propyl-aminium was already applied in a former study for the detection of RO_2 radicals and other oxidized products[23]; the others are used here for the first time. For comparison, analysis was carried out with acetate[22,24–26] and iodide[27,28] as well. The reaction products were observed as clusters with the respective reagent ion as well as deprotonation products in the case of acetate. Figure 2 shows cluster ion traces from a typical experiment of the OH + isoprene reaction using OH radical production via ozonolysis of tetramethylethylene (TME). It should be noted that OH radical formation via O_3 + TME is directly associated with the formation of acetonyl peroxy radicals, $CH_3C(O)CH_2O_2$, representing additional RO_2 radicals in the reaction system[23,29].

Signals of the corresponding masses for the closed-shell products $C_5H_8O_3$ (HPALDs), $C_5H_8O_4$, and $C_4H_8O_5$, as well as for the RO_2 radicals HO-$C_5H_8(O_2)_\alpha O_2$, $\alpha = 0$, 1, and 2, are identified qualitatively in line with the expected product distribution based on recent theoretical and experimental work[12,13], see Fig. 1. Signals of the most abundant products HO-$C_5H_8O_2$, $C_5H_8O_3$, and $C_5H_8O_4$ are already visible from the pure O_3 + isoprene reaction accounting for 5–6% of the maximum signal obtained under conditions of the main OH generation via O_3 + TME. This behavior is in line with the results from modeling, indicating a 5% fraction of OH radicals produced via O_3 + isoprene in the O_3/TME/isoprene system (see the reaction scheme in Supplementary Note 1). There are no indications that signals from pure isoprene ozonolysis influence the product signals attributed to the OH + isoprene reaction. Results from experiments with labeled isoprene, isoprene-1-^{13}C, also confirm the signal assignment based on the signal shift by 1.003 Th.

Other product signals attributed to OH + isoprene products, not given in Fig. 2, indicate the formation of the isomeric hydroxy

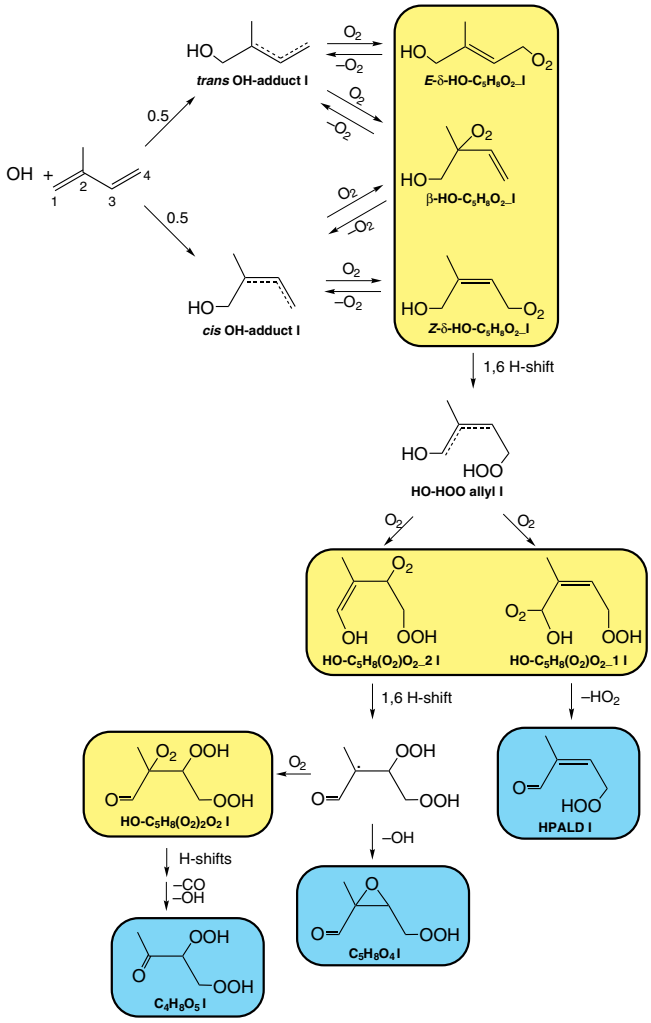

Fig. 1 First reaction steps starting from the OH attack at the 1-position. The given scheme is in line with the current knowledge given in the literature[11–13]. Boxes indicate the products whose corresponding signals have been observed by mass spectrometry. Yellow: RO_2 radicals; blue: closed-shell products. Possible bimolecular RO_2 radical reactions are not shown. Corresponding reaction scheme for the OH attack at the 4-position is given in Supplementary Fig. 1

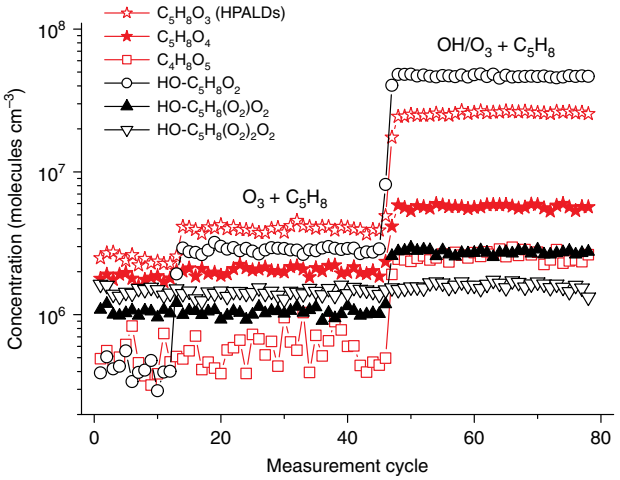

Fig. 2 Signals of selected cluster ion traces from the OH + isoprene reaction. Cluster ion traces attributed to $C_5H_8O_3$, $C_5H_8O_4$, $C_4H_8O_5$, and $HO\text{-}C_5H_8(O_2)_\alpha O_2$, $\alpha = 0$, 1, and 2 are shown depending on the reaction conditions. OH radicals were mainly generated via tetramethylethylene (TME) ozonolysis. Product ionization was carried out by means of hydrazinium, $H_2NNH_3^+$. The background measurement has been done in the presence of isoprene. Ozone was switched on at measurement cycle 13 and TME at measurement cycle 46 starting the main OH generation. It is noteworthy that the $(C_4H_8O_5)H_2NNH_3^+$ signal was influenced by other ions, which probably arise from OH reactions with background impurities, being not corrected here. Reactant concentrations are $[O_3] = 9.4 \times 10^{11}$, $[TME] = 2.0 \times 10^{11}$, and $[isoprene] = 2.5 \times 10^{12}$ molecules cm^{-3} and the reaction time 7.9 s. Stated concentrations represent lower limits; a measurement cycle comprises 60 s data accumulation

hydroperoxides $HO\text{-}C_5H_8OOH$ and probably other $C_5H_{10}O_3$ products, and the accretion products $C_{10}H_{18}O_4$ and $C_{10}H_{18}O_6$. The product with the composition $C_5H_{10}O_2$ is ascribed to $HO\text{-}C_5H_8OH$ formed from $HO\text{-}C_5H_8O_2$ radical dismutation reactions.

Further support especially for the ascertained RO_2 radicals comes from runs applying photolysis of isopropyl nitrite as a second OH radical source, i.e., with OH radical production via $NO + HO_2$[30]. Under these conditions, the RO_2 radicals are reacting with NO forming organic nitrates $RONO_2$ with a yield of up to 0.3[31]. The expected $RONO_2$ signals of the three different $HO\text{-}C_5H_8(O_2)_\alpha O_2$ radicals, $\alpha = 0$, 1, and 2, are visible but with a very weak signal for the highest oxidized $RONO_2$ arising from the RO_2 radical with $\alpha = 2$ (Supplementary Fig. 2). Signals of the three RO_2 radicals and for the closed-shell products featured roughly the same relative abundance among each other as observed in the runs with TME ozonolysis for OH radical production.

Efficiency of product detection and bimolecular pathways. The lack of needed reference substances or of an independent way of defined in-situ product formation makes signal calibration very challenging, especially for RO_2 radicals[32]. Thus, calibration factors are calculated taking into account the following: (i) collision limit of the cluster formation rate from the ion-molecule reaction[22–24,33–36], i.e., reagent ion + product → (product)reagent-ion cluster or via the ligand switch reaction (*X*)reagent ion + product → (product) reagent-ion cluster + *X* (*X* stands for a ligand) and (ii) negligible cluster losses inside the instrument. Concentrations calculated in this way represent lower limits. It is impossible to check the validity of condition (i). However, quantum chemical calculations on the cluster stability were performed to get a measure for the probability that a formed cluster survives the different stages in the mass spectrometer without decomposition as requested in condition (ii).

It is discovered that the different aminium reagent ions and hydrazinium are able to form two hydrogen bonds to all of the products investigated here (see examples in Fig. 3). It is worth noting that all products are bearing at least two oxygen-containing moieties (see Fig. 1). For a selected oxidation product, binding with the reagent ion becomes stronger in the following order: *n*-propyl-aminium < methyl-aminium < hydrazinium. The corresponding clusters formed by iodide as the reagent ion show a distinctly lower stability being qualitatively in line with the experimentally observed lower detection sensitivities in the case of iodide. On the other hand, for acetate the calculations predict strongly bound (product)acetate clusters. The measurements, however, reveal that acetate is a less efficient reagent ion for product detection in this reaction system probably due to a cluster formation rate that is distinctly lower than collision limit,

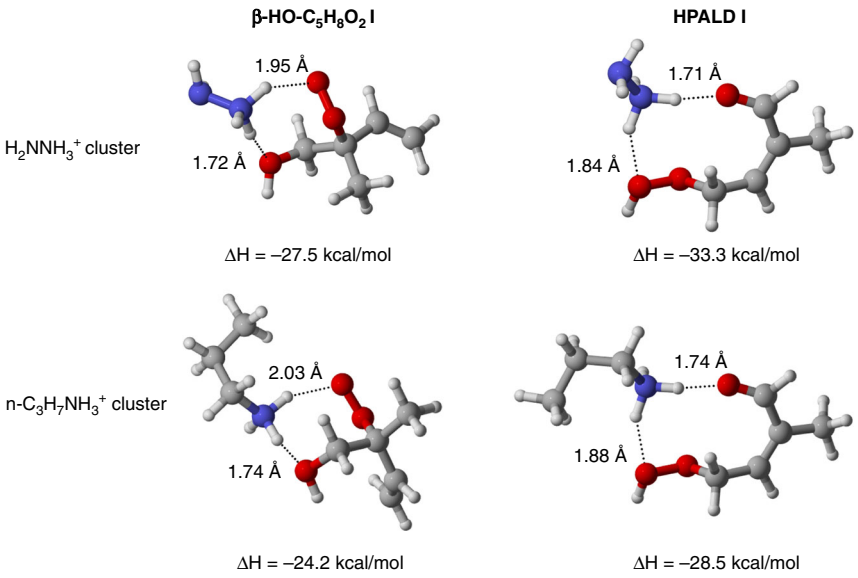

Fig. 3 Structures and formation enthalpies of (product)reagent-ion clusters. Color coding: C = gray, H = white, O = red, N = blue

i.e., condition (i) is probably not fulfilled. Calculated formation enthalpies and free energies of reagent-ion clusters with *Z*-δ- and β-OH-$C_5H_8O_2$ radicals, $C_5H_8O_3$ (HPALDs), and $C_4H_8O_5$ are given in Supplementary Tables 1 and 2.

Product measurements with the six reagent ions (*n*-propyl-, ethyl- or methyl-aminium, hydrazinium, acetate, and iodide) were conducted using a measurement series with TME ozonolysis for OH radical formation varying the ozone concentration in the range $(1.2–95) \times 10^{10}$ molecules cm^{-3} for constant TME and isoprene concentrations of 2.0×10^{11} and 2.5×10^{12} molecules cm^{-3}, respectively. The amount of reacted isoprene increased linearly with rising ozone and subsequently rising OH radical concentrations, reacted isoprene = $(1.7–132) \times 10^7$ and steady-state OH concentration = $(8.5–670) \times 10^3$ molecules cm^{-3} as calculated from a simple reaction scheme. Consecutive OH radical reactions of the first-generation products, which consumed < 0.03% of formed products, can be neglected (see Supplementary Note 1).

HO-$C_5H_8(O_2)_\alpha O_2$ with $\alpha = 0–2$ and $C_5H_8O_3$ (HPALDs). Figure 4 shows the obtained lower limit concentrations of the isomeric RO_2 radicals HO-$C_5H_8(O_2)_\alpha O_2$, $\alpha = 0$, 1, and the HPALDs $C_5H_8O_3$. Considering the three aminium reagent ions and hydrazinium, the detection sensitivity behaves in the following order: *n*-propyl-aminium < ethyl-aminium ≤ methyl-aminium ≤ hydrazinium in line with the trend of the cluster stability from quantum chemical calculations (Supplementary Tables 1 and 2).

In the case of the isomeric HO-$C_5H_8O_2$ radicals (Fig. 4a), the sensitivity differences are distinctly marked in the expected order. Even by applying hydrazinium as the reagent ion, obtained HO-$C_5H_8O_2$ radical concentrations are by a factor of about 15 smaller than the calculated HO-$C_5H_8O_2$ radical concentration from a detailed reaction mechanism. The calculations consider 1,6 H-shift product formation based on the RO_2 radical dynamics given by Teng et al.[13] and the HO-$C_5H_8O_2 + HO_2$ reaction (see Supplementary Note 2). The HO-$C_5H_8O_2$ radicals are bearing only an OH group besides the peroxy moiety and the cluster formation enthalpy of β-HO-$C_5H_8O_2$ radicals, representing the main HO-$C_5H_8O_2$ fraction[12,13], is relatively small compared with the other products (Supplementary Tables 1 and 2). Insufficient cluster stability is most likely the reason for the relatively low detection sensitivity. In this context, NH_4^+ ionization appears to be a more efficient way of HO-$C_5H_8O_2$ radical detection caused by the expected higher (HO-$C_5H_8O_2$)NH_4^+ cluster stability[23,36]. The measurements using iodide and acetate for ionization yield lower values, especially in the latter case with signal intensities close to the detection limit.

The HO-$C_5H_8(O_2)O_2$ lower limit concentrations (Fig. 4b) are within a factor of about two using either hydrazinium, methyl- or ethyl-aminium, or iodide in the ionization process. The good agreement of the results allows the conclusion that HO-$C_5H_8(O_2)O_2$ radicals are measured with close to maximum sensitivity applying these four reagent ions, i.e., the given lower limit concentrations are approaching the "real" concentrations. The additional functional group, most likely an OOH group, causes enhanced detectability of HO-$C_5H_8(O_2)O_2$ radicals due to stronger binding to the reagent ions.

Only very weak signals attributed to HO-$C_5H_8(O_2)_2O_2$ radicals are visible being close to the background level, especially in the case of ionization by the aminium ions and hydrazinium. The resulting lower limit concentrations do not exceed concentrations of 2×10^5 molecules cm^{-3} (Supplementary Fig. 3). It is assumed that further RO_2 radical functionalization gives rise to the formation of a second OOH group in HO-$C_5H_8(O_2)_2O_2$ (Fig. 1 and Supplementary Fig. 1), which causes good detectability also by means of acetate and iodide with close to maximum sensitivity.

The lower limit concentrations obtained for $C_5H_8O_3$, HPALDs, agree well within a factor of 2–3 using hydrazinium or the three aminium ions for ionization (see Fig. 4c). Our signal measured at the exact mass of the ($C_5H_8O_3$)reagent-ion cluster is solely attributed to the HPALDs. Also here, close to maximum sensitivity can be expected especially in the case of hydrazinium and methyl-aminium used as the reagent ions. Further support for efficient HPALD detection comes from the comparison with the data by Teng et al.[13], which account for about half of our maximum HPALD concentrations (see the blue dashed-dotted line in Fig. 4c). Based on end-product analysis in combination with theoretical results, the work by Teng et al.[13] provides comprehensive information on the RO_2 radical dynamics and the HO-$C_5H_8O_2$ isomer-specific product formation needed for reasoned modeling of the reaction system. These authors also

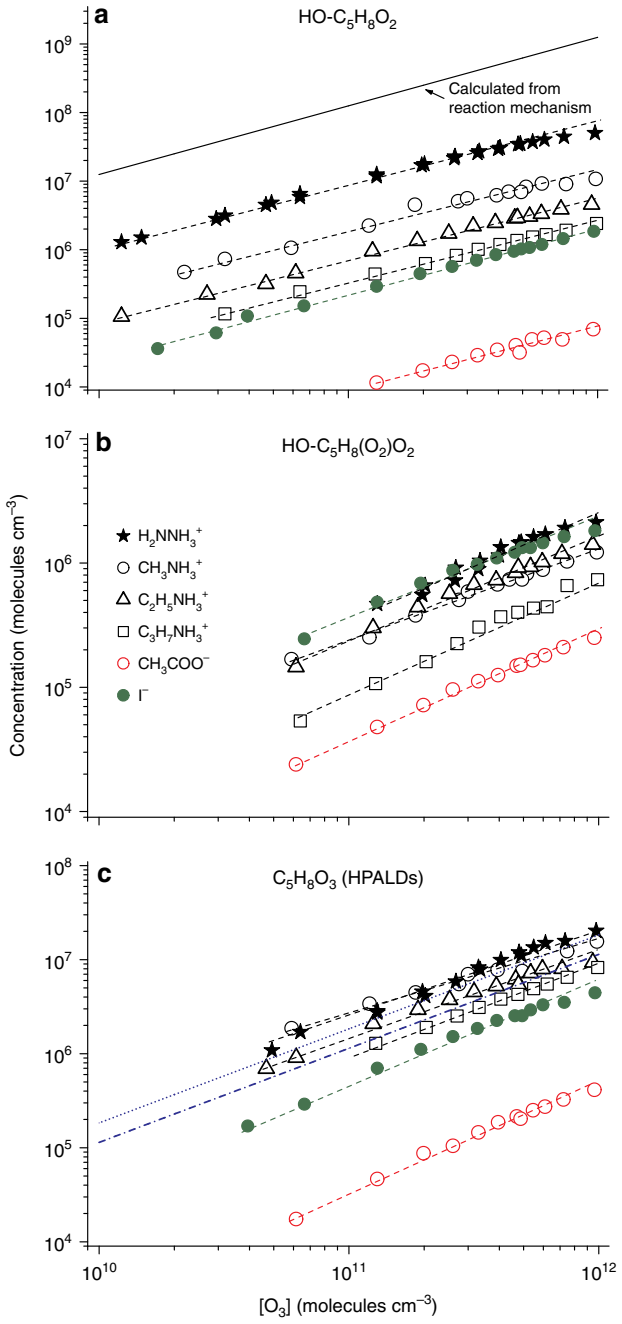

Fig. 4 Lower-limit product concentrations obtained by different ionization schemes. Section **a** shows the results of the HO-$C_5H_8O_2$ radicals, section **b** the HO-$C_5H_8(O_2)O_2$ radicals, and section **c** the data for $C_5H_8O_3$ (HPALDs). In section **c**, the blue dashed-dotted line represents the calculated HPALD data and the blue dotted line the total amount of HPALD and "MW 116," based on Teng et al.[13] using their reaction mechanism and the stated 25% HPALD fraction of the total 1,6 H-shift products[13] (see Supplementary Note 2). Reactant concentrations are $[O_3] = (1.2\text{–}95) \times 10^{10}$, $[TME] = 2.0 \times 10^{11}$ and $[isoprene] = 2.5 \times 10^{12}$ molecules cm^{-3} and the reaction time 7.9 s. Calculated steady-state OH concentrations ranged from 8.5×10^3 to 6.7×10^5 molecules cm^{-3}

reported other, nonspecified "MW 116" products with a 0.61 yield relative to the HPALDs[13], which could have an impact on our HPALD analysis if formed under our conditions. Unfortunately, there is no information on the chemical structure of these "MW 116" products and possible pathways leading to these compounds[13]. Assuming that the exact mass of "MW 116" is consistent with the chemical composition $C_5H_8O_3$, the formation of the first-generation products other than unsaturated C_5 hydroperoxy carbonyls (HPALDs) is mechanistically hard to explain. The total amount of HPALD and "MW 116" by Teng et al.[13] accounts for up to 80% of our HPALD concentrations measured with hydrazinium ionization (see the blue dotted line in Fig. 4c). Other experimental data on non-isomer-specific HPALD formation[18,19] are not directly comparable because of the different bimolecular HO-$C_5H_8O_2$ reactivity and HO-$C_5H_8O_2$ isomer distribution under the different reaction conditions.

$C_5H_8O_4$ and $C_4H_8O_5$. Measurement data for the closed-shell products $C_5H_8O_4$ and $C_4H_8O_5$ from 1,6 H-shift reactions of the Z-δ-HO-$C_5H_8O_2$ radicals are given in the Supplementary Figs. 4 and 5, respectively. Based on the current understanding of the reaction pathways and the expected product structures, $C_5H_8O_4$ and $C_4H_8O_5$ are bearing at least one OOH group and a carbonyl moiety, and possess a similar molecular structure to the HPALDs. The assumed detectability of $C_5H_8O_4$ and $C_4H_8O_5$ with close to maximum sensitivity, such as for the HPALDs, is supported by the strong binding with the reagent ions, as calculated in the case of $C_4H_8O_5$ I (Supplementary Tables 1 and 2).

$C_5H_{10}O_3$. Product formation in the reaction system is inevitably connected with HO_2 radical generation, especially from HPALD production. A further HO_2 radical source is the O_3 + isoprene reaction[37] and additionally we assume an 8% HO_2 yield from O_3 + TME accounting for the pathways not leading to OH radical production (OH yield: 92%[38]). The expected signal of $C_5H_{10}O_3$, attributed to hydroxy hydroperoxides from the HO-$C_5H_8O_2$ + HO_2 reaction via pathway (1), was observed (see Supplementary Fig. 6).

$$\text{HO-C}_5\text{H}_8\text{O}_2 + \text{HO}_2 \rightarrow \text{HO-C}_5\text{H}_8\text{OOH} + \text{O}_2 \qquad (1)$$

Measurements with hydrazinium and methyl-aminium yielded again almost identical results. The comparison with calculated HO-C_5H_8OOH concentrations agreed reasonably with the measurement only for the highest isoprene conversion with $[O_3] = 9.5 \times 10^{11}$ molecules cm^{-3}, calculated $C_5H_{10}O_3$ concentration: 1.6×10^7 and maximum $C_5H_{10}O_3$ measurement: 3.9×10^7 molecules cm^{-3}. Apart from that, the calculations clearly underpredict the measurements. This behavior points to other HO_2 radical sources, not considered yet, or probably to the formation of $C_5H_{10}O_3$ substances other than the hydroxy hydroperoxides. Formation of the second-generation products, such as the dihydroxy epoxides[39], can be neglected due to the small isoprene conversion.

$C_5H_{10}O_2$, $C_{10}H_{18}O_4$, $C_{10}H_{18}O_6$ and other accretion products. Although the reaction conditions were chosen in such a way that the RO_2 radical consumption by bimolecular steps is less important for the RO_2 balance, reaction products from RO_2 self- and cross-reaction become visible, especially for conditions of relatively high isoprene conversion. Figure 5 shows the lower limit concentrations of $C_5H_{10}O_2$ and $C_{10}H_{18}O_4$ along with the HO-$C_5H_8O_2$ radicals measured by hydrazinium ionization and Supplementary Fig. 7 shows the $C_5H_{10}O_2$ measurement data obtained from the different reagent ions. The concentrations of $C_5H_{10}O_2$ and $C_{10}H_{18}O_4$ show a parallel behavior and their slope with rising ozone, and subsequently rising isoprene conversion, is almost twice the slope of the HO-$C_5H_8O_2$ radical concentration (Fig. 5). This behavior is consistent with a bimolecular RO_2 radical reaction leading to $C_5H_{10}O_2$ and $C_{10}H_{18}O_4$. It can be assumed that $C_5H_{10}O_2$ mainly stands for the diol HO-C_5H_8OH

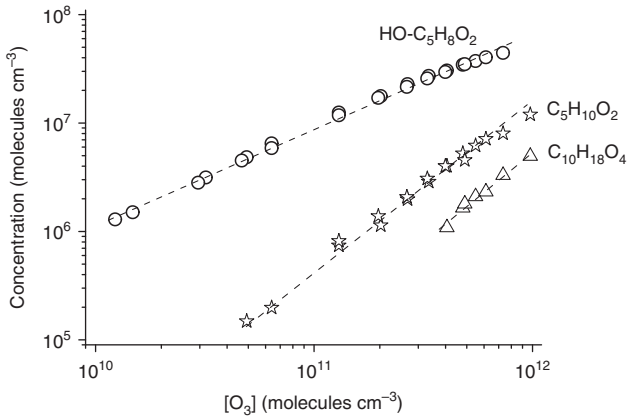

Fig. 5 Lower limit $C_5H_{10}O_2$ and $C_{10}H_{18}O_4$ concentrations compared with the precursor RO_2 radicals. Reactant concentrations are $[O_3] = (1.2–95) \times 10^{10}$, $[TME] = 2.0 \times 10^{11}$ and $[isoprene] = 2.5 \times 10^{12}$ molecules cm^{-3} and the reaction time 7.9 s. Analysis has been carried out by hydrazinium ionization. HO-$C_5H_8O_2$ radical concentrations are underestimated by a factor of about 15

formed via RO_2 radical dismutation reactions[31],

$$\text{HO-C}_5\text{H}_8\text{O}_2 + \text{R'O}_2 \rightarrow \text{HO-C}_5\text{H}_8\text{OH} + \text{R'}(-\text{H}, = \text{O}) + \text{O}_2 \quad (2)$$

where $R'O_2$ represents either an HO-$C_5H_8O_2$ radical or an acetonyl peroxy radical $CH_3C(O)CH_2O_2$. Acetonyl peroxy radicals are formed in the O_3 + TME reaction together with the desired OH radical generation[23,29]. Ruppert and Becker[40] reported the formation of two unsaturated C_5 diols, 2-methyl-3-butene-1,2-diol and 3-methyl-3-butene-1,2-diol, with a total molar yield of 7.1 ± 2.3% from the OH + isoprene reaction conducted in a chamber for low NO_x conditions. The distinctly lower diol yield of < 0.5% from the present study is due to the less efficient bimolecular RO_2 radical reactions under our experimental conditions. Unambiguous identification of the corresponding carbonyl products R′(–H, = O) fails because of the large background signals in the respective range of the mass spectrum. The HO-$C_5H_8O_2$ radical self-reaction forms the accretion product $C_{10}H_{18}O_4$ according to the general accretion pathway $RO_2 + R'O_2 \rightarrow ROOR' + O_2$[23].

$$\text{HO-C}_5\text{H}_8\text{O}_2 + \text{HO-C}_5\text{H}_8\text{O}_2 \rightarrow \text{C}_{10}\text{H}_{18}\text{O}_4 + \text{O}_2 \quad (3)$$

The rate coefficient $k_3 = 6 \times 10^{-13}$ cm^3 $molecule^{-1}$ s^{-1}, $T = (297 \pm 1)$ K, has been estimated in a previous study assuming an uncertainty to be not higher than a factor of 2–3[23]. The measured $C_{10}H_{18}O_4$ concentrations at the residence time t are used to count back the HO-$C_5H_8O_2$ radical concentrations according to $[\text{HO-C}_5\text{H}_8\text{O}_2]_t = (3\ [\text{C}_{10}\text{H}_{18}\text{O}_4]_t/t/k_3)^{0.5}$[23], which are found in good agreement with the calculated HO-$C_5H_8O_2$ data from a detailed reaction mechanism based on the RO_2 radical dynamics given by Teng et al.[13], see Supplementary Note 2 and Supplementary Fig. 8.

For elevated isoprene conversion with $[O_3] > 10^{12}$ molecules cm^{-3} also the formation of $C_{10}H_{18}O_6$ from the RO_2 cross-reaction via pathway (4) becomes detectable (see Fig. 6).

$$\text{HO-C}_5\text{H}_8\text{O}_2 + \text{HO-C}_5\text{H}_8(\text{O}_2)\text{O}_2 \rightarrow \text{C}_{10}\text{H}_{18}\text{O}_6 + \text{O}_2 \quad (4)$$

Further observed accretion products are $C_8H_{14}O_4$ and $C_8H_{14}O_6$ from the cross-reaction of acetonyl peroxy radicals, $CH_3C(O)CH_2O_2$, with HO-$C_5H_8(O_2)_\alpha O_2$, $\alpha = 0$, 1, as well as $C_6H_{10}O_4$ from the $CH_3C(O)CH_2O_2$ self-reaction (Fig. 6). The very good agreement between the results using either hydrazinium or ethyl-aminium ionization suggests that also the accretion products are detected with close to maximum sensitivity.

HO-$C_5H_8O_2$ radical balance. Modeling of the reaction system for $[O_3] = 9.5 \times 10^{11}$, $[TME] = 2.0 \times 10^{11}$ and $[isoprene] = 2.5 \times 10^{12}$ molecules cm^{-3}, and a reaction time 7.9 s reveals an isoprene conversion of 1.322×10^9 and the concentration of the isomeric HO-$C_5H_8O_2$ radicals of 1.265×10^9 molecules cm^{-3}. Calculations were performed based on the data by Teng et al.[13] for the HO-$C_5H_8O_2$ radical dynamics and the 1,6 H-shift reactions including HO-C_5H_8OOH formation via pathway (1) (see the reaction mechanism in Supplementary Note 2). Using the results with hydrazinium ionization, total concentrations of 1,6 H-shift products and HO-C_5H_8OOH, assuming that $C_5H_{10}O_3$ solely stands for the hydroxy hydroperoxides, account for 6.8×10^7 molecules cm^{-3} in reasonable agreement with the modeling results. Additional HO-$C_5H_8O_2$ consuming steps are the accretion product formations with 3.5×10^7 molecules cm^{-3} in total (mainly $C_8H_{14}O_4$ formation from the reaction with $CH_3C(O)CH_2O_2$ radicals) as well as the dismutation reaction with 2.4×10^7 molecules cm^{-3}, twofold the measured $C_5H_{10}O_2$ concentration as a conservative estimate. These bimolecular RO_2 reaction steps together consume < 5% of the calculated HO-$C_5H_8O_2$ radical concentration. It is to be noted that there is no experimental information on the alkoxy radical formation via $RO_2 + R'O_2 \rightarrow RO + R'O + O_2$[31] in our experiments, which is not considered yet in the HO-$C_5H_8O_2$ radical balance. Assuming that alkoxy radical formation accounts for about half of the total product formation from RO_2 radical self- and cross-reactions, i.e., a branching ratio of 0.5 as measured in the case of the HO-$C_2H_4O_2$ self-reaction[31], the experimentally observed and expected bimolecular RO_2 reactions in total consume < 10% of the HO-$C_5H_8O_2$ radicals for the highest isoprene conversion considered here. For lower isoprene conversion, and consequently lower HO-$C_5H_8O_2$ radical concentrations, the bimolecular RO_2 radical reactions are still less important.

Time-dependent product formation. The concentrations of HPALD, $C_5H_8O_4$, and $C_4H_8O_5$ increase in a parallel way among each other with rising reaction time qualitatively in accordance with the behavior of HPALD concentrations (and other isomerization products) as given by the work of Teng et al.[13] (Fig. 7). Measured data for the HO-$C_5H_8(O_2)_\alpha O_2$ radicals with $\alpha = 0$ and 1, which reveal an almost linear increase with time, are depicted in Supplementary Fig. 9. The linear increase of the HO-$C_5H_8O_2$ signal with time confirms that bimolecular RO_2 radical reactions, which become more important with rising RO_2 concentrations, do not significantly influence the HO-$C_5H_8O_2$ radical level. Our time-dependent HPALD concentrations are about twice the values by Teng et al.[13], similar to the findings for changing isoprene conversion at a constant reaction time of 7.9 s (see Fig. 4c). The total amount of HPALD and "MW 116" reported by Teng et al.[13] accounts for 80–90% of our HPALD concentrations, again similar to the behavior obtained from the measurement series with a reaction time of 7.9 s. The formation yields of $C_5H_8O_4$ and $C_4H_8O_5$ relative to HPALD from the present study are 0.20 ± 0.01 and 0.027 ± 0.005, respectively (Supplementary Fig. 10). Although the HPALD results of our study are about twice the data by Teng et al.[13] (Fig. 7), our relative value for $C_5H_8O_4$ is in reasonable agreement with $[C_5H_8O_4]/[\text{HPALDs}] = 0.14$ given by Teng et al.[13]. There is no experimental information on $C_4H_8O_5$ formation up to now in the literature.

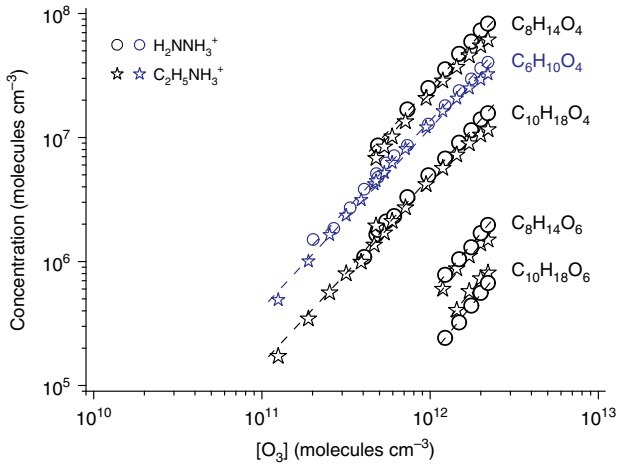

Fig. 6 Accretion product formation from the extended range of isoprene conversion. Reactant concentrations are $[O_3] = (1.2–22) \times 10^{11}$, [TME] = 2.0×10^{11}, and [isoprene] = 2.5×10^{12} molecules cm^{-3} and the reaction time 7.9 s. Analysis has been carried out by hydrazinium and ethyl-aminium ionization. $C_{10}H_{18}O_4$ is formed from the self-reaction of HO-$C_5H_8O_2$ and $C_{10}H_{18}O_6$ from the cross-reaction with HO-$C_5H_8(O_2)O_2$, $C_8H_{14}O_{4,6}$ from the cross-reactions of $CH_3C(O)CH_2O_2$ with HO-$C_5H_8(O_2)_\alpha O_2$, $\alpha = 0$, 1, and $C_6H_{10}O_4$ from the $CH_3C(O)CH_2O_2$ self-reaction. $CH_3C(O)CH_2O_2$ radicals are formed from TME ozonolysis

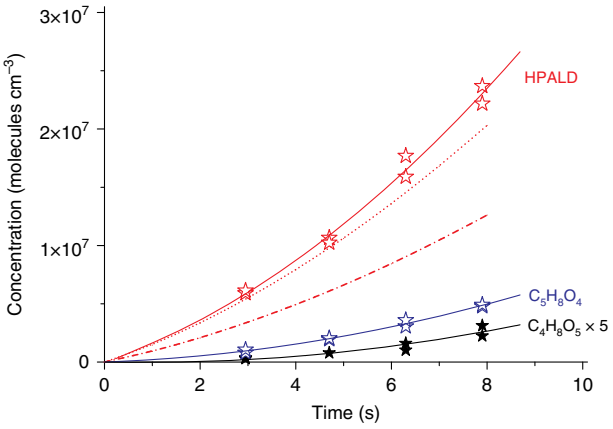

Fig. 7 Time-dependent measurement of closed-shell products. The red stars depict the signal measured at the $(C_5H_8O_3)H_2NNH_3^+$ mass, which is solely attributed to the HPALDs. Analysis was carried out using hydrazinium ionization. Reactant concentrations are $[O_3] = 1.04 \times 10^{12}$, [TME] = 2.0×10^{11}, and [isoprene] = 2.5×10^{12} molecules cm^{-3}. The red dashed-dotted line shows the HPALD concentrations and the red dotted line the total amount of HPALD and "MW 116", based on the work by Teng et al.[13]

1,6 H-shift product distribution. The predominant 1,6 H-shift products from *Z*-δ-HO-$C_5H_8O_2$ radicals detected in the present study are the HPALDs accounting for > 75% of the closed-shell products from RO_2 isomerization. This finding is different from the experimental results by Teng et al.[13] who are stating a HPALD yield of 0.25 regarding the total 1,6 H-shift products. A possible reason for this discrepancy is speculative at the moment. However, it should be noted that these authors investigated a NO_x system, and hydroperoxyacetone and hydroperoxyacetaldehyde, not visible in our experiment, were reported as additional 1,6 H-shift products.[13] Moreover, also the reaction pathways leading to unknown "MW 116" products other than HPALDs, as observed by Teng et al.[13], are unclear up to now. Table 1 compares the fraction of individual 1,6 H-shift products on the total 1,6 H-shift products of the work by Teng et al.[13] with those from the present study. The data given by Teng et al.[13] in Table 1 have been derived by a mass balance deviation. In contrast to that, the data from the present work arise from summing up all detected products.

On the absolute scale, total 1,6 H-shift product concentrations from our experiment amount to about 60% of the Teng et al.[13] results (Fig. 8). The agreement is good taking into account an uncertainty of a factor of two in our case. Predicted total 1,6 H-shift products from the theoretical work by Peeters et al.[12], however, are higher by a factor of about 7 compared with our findings.

The data given by Peeters et al.[12] currently represent the base of the OH + isoprene subsystem of the Master Chemical Mechanism, MCM v3.3.1.[41]. Peeters et al.[12] and Teng et al.[13] use a different set of kinetic parameters for description of the RO_2 radical processes resulting in different concentration profiles of the individual RO_2 species and the 1,6 H-shift products, as exemplarily shown in Supplementary Figs 11 and 12 for our conditions. For clearly higher reaction times than in our experiment, $t \geq 50$ s, calculated total 1,6 H-shift product concentrations are within a factor of two based on the data by Peeters et al.[12] and Teng et al.[13] (Supplementary Fig. 12). Expected total 1,6 H-shift product yield in forestlands with the highest isoprene emission and a bimolecular RO_2 reactivity of about 0.02 s^{-1} is 0.28 using the data by Peeters et al.[12] and 0.16 based on the work by Teng et al.[13], both within a factor of 2 (Supplementary Fig. 13). The bimolecular RO_2 reactivity of about 0.02 s^{-1} considers NO and HO_2 radical concentrations of 5×10^8 and 1×10^9 molecules cm^{-3}, respectively, as measured in the tropical forest[42]. For somewhat lower NO and HO_2 radical levels and a supposed bimolecular RO_2 reactivity of 0.005 s^{-1}, the total 1,6 H-shift product yield reaches a value of up to 0.5, demonstrating the importance of RO_2 isomerization steps for the first-generation products from OH + isoprene for pristine reaction conditions (Supplementary Fig. 13). The experiments of this study and the modeling calculations were conducted for a temperature of (297 ± 1) K. Higher temperatures are expected to significantly enhance the rate of RO_2 radical isomerization steps, whereas bimolecular RO_2 radical reactions are less temperature dependent[43]. Thus, the importance of 1,6 H-shift product formation is increasing with rising temperature and vice versa as shown for HPALD generation from a flow tube experiment[19].

HPALD, $C_5H_8O_4$, and $C_4H_8O_5$ formation is connected with equal-molar HO_x recycling being important for the HO_x budget in isoprene-dominated forestlands[42].

Discussion

Within the present work, direct observation of the first oxidation products from OH + isoprene with special attention to the RO_2 isomerization products is reported. Reaction conditions were chosen in such a way that bimolecular RO_2 reactions, with exception of NO + RO_2 in a few runs, did not significantly influence the RO_2 radical concentrations. The isomeric RO_2 radicals HO-$C_5H_8(O_2)_\alpha O_2$ with $\alpha = 0$, 1, and 2 were followed together with their closed-shell products HPALD, $C_5H_8O_4$, and $C_4H_8O_5$ formed via unimolecular pathways. The products, with the exception of the primarily formed HO-$C_5H_8O_2$ radicals, are most likely measured with close to maximum sensitivity, i.e., analysis is approaching the "real" concentrations with an uncertainty by a factor of about two due to the expected uncertainty of the calculated calibration factor.

Table 1 Observed 1,6 H-shift products and their fraction on the total 1,6 H-shift products (%)

Product	Teng et al.[13a]	This work[b]
HPALDs, $C_5H_8O_3$	25	76[c]
"MW 116" (other than HPALDs)	15	—[c]
"MW 132", $C_5H_8O_4$	3.5	15
Hydroperoxyacetaldehyde	8.2	ND
Hydroperoxyacetone	16	ND
$C_4H_8O_5$	ND	2.1
HO-$C_5H_8(O_2)O_2$	ND	5.5
HO-$C_5H_8(O_2)_2O_2$	ND	0.8

[a]Stated products account for 68% of the total 1,6 H-shift products
[b]From time-dependent measurements as given in Fig. 7
[c]The signal measured at the exact mass of $C_5H_8O_3$ is solely attributed to the HPALDs
ND not detected

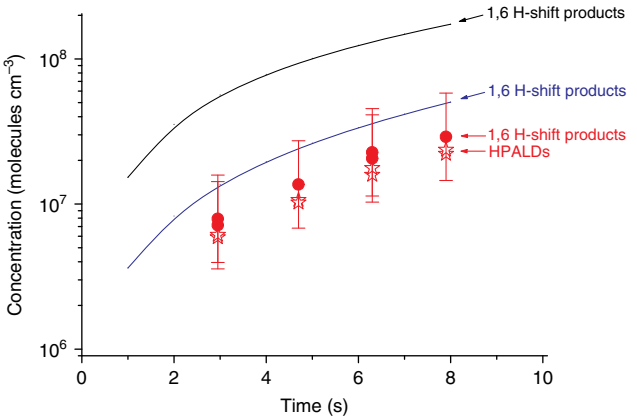

Fig. 8 Comparison of the total 1,6 H-shift product concentrations. Experimental results of the present study are depicted in red. Our signal measured at the product mass of $C_5H_8O_3$ is solely attributed to the HPALDs. Error bars given for the total 1,6 H-shift products stand for the uncertainty by a factor of two for the lower limit concentrations. The blue full line shows the total 1,6 H-shift concentration based on the work by Teng et al.[13] (Supplementary Note 2). The black full line shows the total 1,6 H-shift concentration based on the work by Peeters et al.[12] (Supplementary Note 3)

Furthermore, the accretion products $C_{10}H_{18}O_4$ and $C_{10}H_{18}O_6$, as well as $C_5H_{10}O_2$, most likely HO-C_5H_8OH, have been detected from RO_2 self- and cross-reactions. Products with the composition $C_5H_{10}O_3$ were at least partly attributed to the isomeric hydroxy hydroperoxides HO-C_5H_8OOH.

Our results suggest that the formation of HO-$C_5H_8(O_2)_2O_2$ radicals, and subsequently $C_4H_8O_5$, is overvalued in the MCM v3.3.1[41]. $C_4H_8O_5$ represents only a minor product accounting only for 2–3% of the total closed-shell products formed via 1,6 H-shift of *Z*-δ-HO-$C_5H_8O_2$ radicals. MCM v3.3.1. describes HPALD and $C_4H_8O_5$ formation with the same yields for conditions of low bimolecular RO_2 reactivity, as present in remote areas as well as in our experiment[41]. Apart from that, the formation of $C_5H_8O_4$ as another important 1,6 H-shift product beside the HPALDs should be considered in atmospheric modeling. The present study also indicates that the formation of highly oxygenated molecules (HOMs) as the first-generation products from OH + isoprene is less important being qualitatively in line with a molar HOM yield of about 0.03% regarding the reacted isoprene obtained for similar reaction conditions as applied here[44]. A recently predicted molar HOM yield of up to 11% for conditions of a bimolecular RO_2 reactivity of 0.01 s^{-1}[45] is in contradiction to our experimental findings as well as to the low formation of secondary organic aerosol mass from the first-generation OH + isoprene products observed in smog chamber experiments[46,47].

Methods

Flow system. Experiments have been performed in a free-jet flow system[22,23,48] at a pressure of 1 bar of purified air and a temperature of (297 ± 1) K. Reaction times were in the range 3.0–7.9 s. The flow system consists of an outer tube (length: 200 cm, inner diameter: 16 cm) and a moveable inner tube (outer diameter: 9.5 mm) with a nozzle of 3 mm inner diameter. Ozone premixed with air (5 L min^{-1}, STP) is injected through the inner tube into the main gas stream (95 L min^{-1} at standard temperature and pressure, STP), which contains the other reactants, TME and isoprene in most cases, diluted in air. The gas velocity at the nozzle outflow, nozzle: 15.9 m s^{-1}, main flow: 0.13 m s^{-1}, and the nozzle geometry ensure rapid reactant mixing. Effective reaction times between the nozzle outflow and the sampling point were experimentally determined by means of a "chemical clock", i.e., by measuring ozone disappearance in the presence of excess of TME[48].

OH radicals have been generated primarily via ozonolysis of TME[29]. Photolysis of isopropyl nitrite was used as an alternative OH radical source[30]. The photolysis was carried out downstream the mixing point of the gas streams by means of 8 NARVA 36 W Blacklight Blue lamps.

Reactant concentrations were in the range: $[O_3] = (1.2–230) \times 10^{10}$, $[TME] = 2.0 \times 10^{11}$, $[isoprene] = (5.0–25) \times 10^{11}$, and $[isoprene\text{-}1\text{-}^{13}C] = 2.5 \times 10^{12}$ molecules cm^{-3}. Isopropyl nitrite concentrations in the photolysis experiments were $(3.5–104) \times 10^{10}$ molecules cm^{-3}.

Product measurements. The detection of RO_2 radicals and closed-shell products has been conducted by a CI-APi-TOF (chemical ionization–atmospheric pressure interface–time-of-flight) mass spectrometer (Airmodus, Tofwerk) that sampled from the center flow of the flow system with a rate of 10 L min^{-1} (STP). The resolving power of the mass spectrometer was > 3000 Th/Th. Ionization was carried out at atmospheric pressure using a Boulder-type inlet system[49]. Used reagent ions were protonated *n*-propyl-, ethyl- or methylamine, protonated hydrazine, acetate, or iodide. All products including the RO_2 radicals, "prod", were detected as a cluster with the reagent ion.

$$(X)_mYH^+ + \mathrm{prod} \rightarrow (\mathrm{prod})YH^+ + m\,X;\ m = 0, 1 \quad (5)$$

In addition, deprotonation products have been considered in the case of acetate. A comparison of the calculated and measured masses of product clusters, (prod)$H_2NNH_3^+$, is given in Supplementary Table 3.

Reagent ions that consist of different protonated amines or hydrazine YH^+ can cluster with ligands $(X)_m$, where *X* stands for H_2O or *Y*. (Product)reagent-ion cluster formation in reaction (5) proceeds at every collision if the ligand switch reaction is exothermic[50]. We calculated the formation enthalpies of (product) reagent-ion clusters (Fig. 3, Supplementary Table 1) revealing that YH^+ forms strongly bound clusters with the products (e.g., (HPALD I)$H_2NNH_3^+$ with 33.3 kcal mol^{-1}). McNary and Armentroud[51] recently investigated experimentally the bond energy of protonated hydrazine water clusters at 0 K and compared them with literature values of amine water clusters. According to that, $H_2NNH_3^+$ is bound to water with 16.4 kcal mol^{-1} and $CH_3NH_3^+$ with 17.8 kcal mol^{-1}. We calculated the corresponding binding enthalpies for $H_2NNH_3^+$, $CH_3NH_3^+$, and n-$C_3H_7NH_3^+$ at 298 K with 19.2, 17.3, and 16.0 kcal mol^{-1}, respectively, in good agreement with the range of bond energies obtained at 0 K[51]. Therefore, the ligand switch reaction (5) is exothermic and fast for all products of OH + isoprene including the RO_2 radicals. The rather strong binding of the product ion clusters (prod)YH^+ is important to prevent the clusters from being lost in collision-induced dissociation (CID) in the APi-TOF. In contrast, weakly bound clusters such as the reagent ions $(X)_mYH^+$ present in the CI region are lost by CID in the APi-TOF. That is the reason why $(H_2O)YH^+$ was not detected in the present experiments. In our previous study using $(X)_mNH_4^+$ cluster ions only rather weak $(H_2O)NH_4^+$ signals have been recorded in the NH_4^+-CI3-TOF instrument running at 80 mbar and using softest injection energies in the quadrupole ion transfer region[36].

In the case of acetate and AcH ≡ acetic acid,

$$\begin{aligned}(\mathrm{AcH})_nCH_3COO^- + \mathrm{prod} &\rightarrow \mathrm{prod} - CH_3COO^- + n\,\mathrm{AcH};\\ &\rightarrow (\mathrm{prod} - \mathrm{H})^- + (n+1)\mathrm{AcH};\ n = 0, 1, 2\end{aligned} \quad (6)$$

and for iodide,

$$(H_2O)_nI^- + \mathrm{prod} \rightarrow (\mathrm{prod})I^- + n\,H_2O;\ n = 0, 1 \quad (7)$$

possible ionization schemes have been discussed in the literature[25–28].

Reagent ion formation. The reagent ions have been generated in a 35 L min^{-1} (STP) sheath flow of purified air or nitrogen (in the case of iodide) from an appropriate precursor compound after ionization with a ^{241}Am source. Formed ions from the sheath flow were guided into the sample flow by an electric field without mixing of both gas streams.

In the case of ionization by acetate, a flow of 1–2 ml min^{-1} (STP) air over an acetic acid sample was added to the sheath flow forming the reagent ions $(CH_3COOH)_mCH_3COO^-$, $m = 0, 1, 2$.

In the case of iodide, tert.-butyl iodide premixed in a flask from a gas-metering unit was added to the sheath flow resulting in a tert.-butyl iodide concentration of 8×10^{10} molecules cm^{-3}. The only detected reagent ion was I^-. I_3^- was measureable in small traces.

Aminium reagent ions, protonated *n*-propyl-, ethyl-, or methylamine were generated from the corresponding amines using amine concentrations of $(2.3–3.5) \times 10^{11}$ molecules cm^{-3} in the sheath gas flow that had a relative humidity of about 1%. The amine samples were taken from a gas mixture in helium produced from a gas-metering unit. Tetrahydrofuran (THF) was added to the sheath flow with a concentration of 1×10^{13} molecules cm^{-3} in the case of methyl-aminium, to enhance the reagent-ion production. The enhancement is obviously caused by the proton transfer reaction of easily formed (THF)-H^+ with CH_3NH_2 due to the higher proton affinity[52]. Detected reagent ions were the naked aminium ions, i.e., $C_3H_7NH_3^+$, $C_2H_5NH_3^+$, or $CH_3NH_3^+$, with exception of the *n*-propyl aminium system where $(C_3H_7NH_2)C_3H_7NH_3^+$ was visible to a lesser amount.

For the formation of hydrazinium ions, a flow of 1 ml min^{-1} (STP) air over a sample of hydrazine monohydrate, 64–65% N_2H_4, was added to the sheath flow that contained 1×10^{13} molecules cm^{-3} of THF for enhanced $H_2NNH_3^+$ production. The only detectable reagent ion was $H_2NNH_3^+$.

Determination of lower limit concentrations. RO_2 radicals and closed-shell products, all termed in the following "prod", were detected as clusters with the respective reagent ions, (prod)reagent-ion. Their concentrations were determined according to equation (8):

$$[\mathrm{prod}] = \mathrm{f}\frac{(\mathrm{prod})\mathrm{reagent} - \mathrm{ion}}{[\mathrm{reagent\ ion}]} \quad (8)$$

The quantities in equation (8) are the measured signal intensities. The "[reagent ion]" comprises the sum of the signal intensities of $(CH_3COOH)_mCH_3COO^-$, $m = 0$, 1, 2 in the case of acetate and $(C_3H_7NH_2)_nC_3H_7NH_3^+$, $n = 0$, 1 in the case of *n*-propyl-aminium. Duty cycle correction is applied to compensate for the mass-dependent transmission of the TOF mass spectrometer[53,54]. According to that the signal strengths were corrected with respect to the reagent ions at their nominal mass. For instance, in the case of acetate with respect to CH_3COO^- at nominal 59 Th are the duty cycle corrected counts per second of product i $\mathrm{dcps(i)} = \mathrm{cps(i)}\sqrt{\frac{59}{m_i}}$.

The lower limit value of the calibration factor f in equation (8) can be calculated considering the ion-molecule reaction in the CI-inlet, $f = 1/(k \times t \times f_{\mathrm{inlet}})$[55,56], where k is the rate coefficient of the ion-molecule reaction, t the reaction time, and f_{inlet} considers the "prod" loss in the sampling tube. The rate coefficient k is set to $(2–3) \times 10^{-9}$ cm^3 $molecule^{-1}$ s^{-1}, typical for ion-molecule reactions close to the collision limit[57,58]. Considering a 12% diffusion loss of "prod" in the short sampling tube (diffusion controlled wall loss for an assumed diffusion coefficient $D = 0.08$ cm^2 s^{-1}), $f_{\mathrm{inlet}} = 0.88$, and a reaction time of the ion-molecule reaction $t = 0.2–0.3$ s, $f_{\mathrm{calc}} = (1.3–2.8) \times 10^9$ molecules cm^{-3} follows. The only reliable absolute calibration in our system at the moment is that used for sulfuric acid detection via $H_2SO_4 + (HNO_3)_nNO_3^-$, $n = 0$, 1, 2, 3, with a calibration factor $f_{\mathrm{H2SO4,exp}} = 1.85 \times 10^9$ molecules cm^{-3}[59]. This value is in good agreement with the range of f_{calc}. The calibration factor f in equation (8) was set equal to $f_{\mathrm{H2SO4,exp}}$, to use a defined value and not a range. The uncertainty of the lower limit "prod" concentrations determined according to equation (8) is assumed to be not higher than a factor of two due to the expected uncertainty of the used calibration factor f, i.e., $f_{\mathrm{H2SO4,exp}} = 1.85 \times 10^9$ compared with the range of $f_{\mathrm{calc}} = (1.3–2.8) \times 10^9$ molecules cm^{-3}, and possible inaccuracy connected with the duty cycle correction.

Computational methods. The stability of the ion-molecule clusters, including the hydrated reagent-ion clusters, was modeled by calculating the formation of free energies and enthalpies of the clusters. The conformer sampling and computational methods were similar to those used by Hyttinen et al.[60,61]. The conformer sampling of the sample molecules and ion-molecule clusters was done using the Spartan '14 program[62]. A systematic conformer sampling algorithm with Merck Molecular Force Field molecular mechanics optimization were used to obtain the initial sets of conformers. All conformers were then optimized at the B3LYP/6–31 + G* level of theory and ultrafine integration grid using Gaussian 09[63]. Final geometry optimizations and harmonic frequencies, also with ultrafine integration grid, were calculated for all conformers within 2 kcal mol^{-1} from the lowest electronic energy conformer at the ωB97X-D/aug-cc-pVTZ (aug-cc-pVTZ-PP for I) level of theory. Final single-point electronic energies were calculated at the DLPNO-CCSD(T)/def2-QZVPP level of theory using the corresponding auxiliary set and tight PNO settings, implemented in the Orca program[64], version 4.0.0.2.

Data availability

All relevant data supporting the findings of this study are available within the article and the Supplementary Information, and from the corresponding author upon reasonable request.

Received: 28 September 2018 Accepted: 30 January 2019
Published online: 21 February 2019

References

1. Goldstein, A. H. & Galbally, I. E. Known and unexplored organic constituents in the Earth's atmosphere. *Environ. Sci. Technol.* **41**, 1514–1521 (2007).
2. Sindelarova, K. et al. Global data set of biogenic VOC emissions calculated by the MEGAN model over the last 30 years. *Atmos. Chem. Phys.* **14**, 9317–9341 (2014).
3. Arneth, A. et al. Terrestrial biogeochemical feedbacks in the climate system. *Nat. Geosci.* **3**, 525–532 (2010).
4. Seinfeld, J. H. & Pandis, S. N. Atmospheric Chemistry and Physics: From Air Pollution to Climate Change (Wiley, New York, 1998).
5. Zimmerman, P. R., Greenberg, J. P. & Westberg, C. E. Measurements of atmospheric hydrocarbons and biogenic emission fluxes in the Amazon boundary layer. *J. Geophys. Res.* **93**, 1407–1416 (1988).
6. Fehsenfeld, F. et al. Emissions of volatile organic compounds from vegetation and the implications for atmospheric chemistry. *Glob. Biogeochem. Cy.* **6**, 389–430 (1992).
7. Lee, S.-H. et al. Isoprene suppression of new particle formation: potential mechanisms and implications. *J. Geophys. Res. Atmos.* **121**, 14621–14635 (2016).
8. Wennberg, P. O. et al. Gas-phase reactions of isoprene and its major oxidation products. *Chem. Rev.* **118**, 3337–3390 (2018).
9. Jenkin, M. E. & Hayman, G. D. Kinetics of reactions of primary, secondary and tertiary β-hydroxy peroxyl radicals. *J. Chem. Soc. Faraday Trans.* **91**, 1911–1922 (1995).
10. Morgan, C. A., Pilling, M. J., Tulloch, J. M., Ruiz, R. P. & Bayes, K. D. Direct determination of the equilibrium constant and thermodynamic parameters for the reaction $C_3H_5 + O_2 \rightarrow\leftarrow C_3H_5O_2$. *J. Chem. Soc. Faraday Trans. 2* **78**, 1323–1330 (1982).
11. Peeters, J., Nguyen, T. L. & Vereecken, L. HO_x radical regeneration in the oxidation of isoprene. *Phys. Chem. Chem. Phys.* **11**, 5935–5939 (2009).
12. Peeters, J., Müller, J.-F., Stavrakou, T. & Nguyen, T. L. Hydroxyl radical recycling in isoprene oxidation driven by hydrogen bonding and hydrogen tunneling: the upgraded LIM1 mechanism. *J. Phys. Chem. A* **118**, 8625–8643 (2014).
13. Teng, A. P., Crounse, J. D. & Wennberg, P. O. Isoprene peroxy radical dynamics. *J. Am. Chem. Soc.* **139**, 5367–5377 (2017).
14. Jenkin, M. E., Boyd, A. A. & Lesclaux, R. Peroxy radical kinetics resulting from the OH-initiated oxidation of 1,3-butadiene, 2,3-dimethyl-1,3-butadiene and isoprene. *J. Atmos. Chem.* **29**, 267–298 (1998).
15. Zhang, D., Zhang, R., Church, C. & North, S. W. Experimental study of hydroxyalkyl peroxy radicals from OH-initiated reactions of isoprene. *Chem. Phys. Lett.* **343**, 49–54 (2001).
16. Medeiros, D. J., Blitz, M. A., James, L., Speak, T. H. & Seakins, P. W. Kinetics of the reaction of OH with isoprene over a wide range of temperature and pressure including direct observation of equilibrium with the OH adducts. *J. Phys. Chem. A* **122**, 7239–7255 (2018).
17. Hermans, I., Müller, J. F., Nguyen, T. L., Jacobs, P. A. & Peeters, J. Kinetics of alpha-hydroxy-alkylperoxyl radicals in oxidation processes. HO_2*-initiated oxidation of ketones/aldehydes near the tropopause. *J. Phys. Chem. A* **109**, 4303–4311 (2005).
18. Crounse, J. D., Paulot, F., Kjaergaard, H. G. & Wennberg, P. O. Peroxy radical isomerization in the oxidation of isoprene. *Phys. Chem. Chem. Phys.* **13**, 13607–13613 (2011).
19. Berndt, T. Formation of carbonyls and hydroperoxyenals (HPALDs) from the OH radical reaction of isoprene for low-NOx conditions: influence of temperature and water vapour content. *J. Atmos. Chem.* **69**, 253–272 (2012).
20. Peeters, J. & Nguyen, T. L. Unusually fast 1,6-H shifts of enolic hydrogens in peroxy radicals: Formation of the first-generation C_2 and C_3 carbonyls in the oxidation of isoprene. *J. Phys. Chem. A* **116**, 6134–6141 (2012).
21. Da Silva, G., Graham, C. & Wang, Z.-F. Unimolecular β-hydroxyperoxy radical decomposition with OH recycling in the photochemical oxidation of isoprene. *Environ. Sci. Technol.* **44**, 250–256 (2010).
22. Berndt, T. et al. Hydroxyl radical-induced formation of highly oxidized organic compounds. *Nat. Commun.* **7**, 13677 (2016).
23. Berndt, T. et al. Accretion product formation from self- and cross-reactions of RO_2 radicals in the atmosphere. *Angew. Chem. Int. Ed.* **57**, 3820–3824 (2018).

24. Berndt, T., Herrmann, H., Sipilä, M. & Kulmala, M. Highly oxidized second-generation products from the gas-phase reaction of OH radicals with isoprene. *J. Phys. Chem. A* **120**, 10150–10159 (2016).
25. Bertram, T. H. et al. A field-deployable, chemical ionization time-of-flight mass spectrometer. *Atmos. Meas. Tech.* **4**, 1471–1479 (2011).
26. Aljawhary, D., Lee, A. K. Y. & Abbatt, J. P. D. High-resolution chemical ionization mass spectrometry (ToF-CIMS): application to study SOA composition and processing. *Atmos. Meas. Tech.* **6**, 3211–3224 (2013).
27. Huey, L. G., Hanson, D. R. & Howard, C. J. Reactions of SF_6^- and I^- with atmospheric trace gases. *J. Phys. Chem.* **99**, 5001–5008 (1995).
28. Lee, B. H. et al. An iodide-adduct high-resolution time-of-flight chemical-ionization mass spectrometer: application to atmospheric inorganic and organic compounds. *Environ. Sci. Technol.* **48**, 6309–6317 (2014).
29. Kroll, J. H., Sahay, S. R., Anderson, J. G., Demerjian, K. L. & Donahue, N. M. Mechanism of HO_x formation in the gas-phase ozone-alkene reaction. 2. Prompt versus thermal dissociation of carbonyl oxides to form OH. *J. Phys. Chem. A* **105**, 4446–4457 (2001).
30. Raff, J. D. & Finlayson-Pitts, B. J. Hydroxyl radical quantum yields from isopropyl nitrite photolysis in air. *Environ. Sci. Technol.* **44**, 8150–8155 (2010).
31. Orlando, J. J. & Tyndall, G. S. Laboratory studies of organic peroxy radical chemistry: an overview with emphasis on recent issues of atmospheric significance. *Chem. Soc. Rev.* **41**, 6294–6317 (2012).
32. Nozière, B. & Hanson, D. R. Speciated monitoring of gas-phase organic peroxy radicals by chemical ionization mass spectrometry: cross-reactions between CH_3O_2, $CH_3(CO)O_2$, $(CH_3)_3CO_2$, and c-$C_6H_{11}O_2$. *J. Phys. Chem. A* **121**, 8453–8464 (2017).
33. Mackay, G. I. & Bohme, D. K. Proton-transfer reactions in nitromethane at 297K. *Intern. J. Mass Spectrom. Ion Phys.* **26**, 327–343 (1978).
34. Viggiano, A. A., Seeley, J. V., Mundis, P. L., Williamson, J. S. & Morris, A. M. Rate constants for the reactions of $XO_3^-(H_2O)_n$ (X = C, HC, and N) and $NO_3^-(HNO_3)_n$ with H_2SO_4: Implications for atmospheric detection of H_2SO_4. *J. Phys. Chem. A* **101**, 8275–8278 (1997).
35. Mackay, G. I., Tanner, S. D., Hopkinson, A. C. & Bohme, D. K. Gas-phase proton-transfer reactions of the hydronium ion at 298°K. *Can. J. Chem.* **57**, 1518–1523 (1979).
36. Hansel, A., Scholz, W., Mentler, B., Fischer, L. & Berndt, T. Detection of RO_2 radicals and other products from cyclohexene ozonolysis with NH_4^+ and acetate chemical ionization mass spectrometry. *Atmos. Environ.* **186**, 248–255 (2018).
37. Malkin, T. L., Goddard, A., Heard, D. E. & Seakins, P. W. Measurements of OH and HO_2 yields from the gas phase ozonolysis of isoprene. *Atmos. Chem. Phys.* **10**, 1441–1459 (2010).
38. Berndt, T. & Böge, O. Formation of phenol and carbonyls from the atmospheric reaction of OH radicals with benzene. *Phys. Chem. Chem. Phys.* **8**, 1205–1214 (2006).
39. Paulot, F. et al. Unexpected epoxide formation in the gas-phase photooxidation of isoprene. *Science* **325**, 730–733 (2009).
40. Ruppert, L. & Becker., K.-H. A product study of the OH radical-initiated oxidation of isoprene: formation of C_5-unsaturated diols. *Atmos. Environ.* **34**, 1529–1542 (2000).
41. Jenkin, M. E., Young, J. C. & Rickard, A. R. The MCMv3.3. 1 degradation scheme for isoprene. *Atmos. Chem. Phys.* **15**, 11433–11459 (2015).
42. Lelieveld, J. et al. Atmospheric oxidation capacity sustained by a tropical forest. *Nature* **452**, 737–740 (2008).
43. Praske, E. et al. Atmospheric autoxidation is increasingly important in urban and suburban North America. *Proc. Natl Acad. Sci. USA* **115**, 64–69 (2018).
44. Jokinen, T. et al. Production of extremely low volatile organic compounds from biogenic emissions: Measured yields and atmospheric implications. *Proc. Natl Acad. Sci. USA* **112**, 7123–7128 (2015).
45. Wang, S., Riva, M., Yan, C., Ehn, M. & Wang, L. Primary formation of highly oxidized multifunctional products in the OH-initiated oxidation of isoprene. A combined theoretical and experimental study. *Environ. Sci. Technol.* **52**, 12255–12264 (2018).
46. Kroll, J. H., Ng, N. L., Murphy, S. M., Flagan, R. C. & Seinfeld, J. H. Secondary organic aerosol formation from isoprene photooxidation. *Environ. Sci. Technol.* **40**, 1869–1877 (2006).
47. Ng, N. L. et al. Contribution of first- versus second-generation products to secondary organic aerosols formed in the oxidation of biogenic hydrocarbons. *Environ. Sci. Technol.* **40**, 2283–2297 (2006).
48. Berndt, T. et al. Kinetics of the unimolecular reaction of CH_2OO and the bimolecular reactions with the water monomer, acetaldehyde and acetone under atmospheric conditions. *Phys. Chem. Chem. Phys.* **17**, 19862–19873 (2015).
49. Eisele, F. L. & Tanner, D. J. Ion-assisted tropospheric OH measurements. *J. Geophys. Res.* **96**, 9295–9308 (1991).
50. Viggiano, A. A., Dale, F. & Paulson, J. F. Proton transfer reactions of $H^+(H_2O)_{n=2-11}$ with methanol, ammonia, pyridine, acetonitrile, and acetone. *J. Chem. Phys.* **88**, 2469–2477 (1989).
51. McNary, C. P. & Armentroud, P. B. Threshold collision-induced dissociation of protonated hydrazine and dimethylhydrazine clustered with water. *J. Chem. Phys.* **145**, 214311 (2016).
52. Hunter, E. P. & Lias, S. G. Evaluated gas phase basicity and proton affinities of molecules: an update. *J. Phys. Chem. Ref. Data* **27**, 413–656 (1998).
53. Breitenlechner, M. et al. PTR3: an instrument for studying the lifecycle of reactive organic carbon in the atmosphere. *Anal. Chem.* **89**, 5824–5831 (2017).
54. Junninen, H. et al. A high-resolution mass spectrometer to measure atmospheric ion composition. *Atmos. Meas. Tech.* **3**, 1039–1053 (2010).
55. Ehn, M. et al. A large source of low-volatility secondary organic aerosol. *Nature* **506**, 476–479 (2014).
56. Berresheim, H., Elste, T., Plass-Dülmer, C., Eisele, F. L. & Tanner, D. J. Chemical ionization mass spectrometer for long-term measurements of atmospheric OH and H_2SO_4. *Int. J. Mass Spectrom.* **202**, 91–109 (2000).
57. Viggiano, A. A., Seelev, J. V., Mundis, P. L., Williamson, J. S. & Morris, R. A. Rate constants for the reaction of $XO_3^-(H_2O)_n$ (X = C, HC, and N) and $NO_3^-(HNO_3)_n$ with H_2SO_4: Implications for atmospheric detection of H_2SO_4. *J. Phys. Chem. A* **101**, 8275–8278 (1997).
58. Mackay, G. I. & Bohme, D. K. Proton-transfer reactions in nitromethane at 297 K. *Intern. J. Mass Spectrom. Ion Phys.* **26**, 327–343 (1978).
59. Berndt, T. et al. H_2SO_4 formation from the gas-phase reaction of stabilized Criegee Intermediates with SO_2: Influence of water vapour content and temperature. *Atmos. Environ.* **89**, 603–612 (2014).
60. Hyttinen, N., Rissanen, M. P. & Kurtén, T. Computational comparison of acetate and nitrate chemical ionization of highly oxidized cyclohexene ozonolysis intermediates and products. *J. Phys. Chem. A* **120**, 2172–2179 (2017).
61. Hyttinen, N. et al. Computational comparison of different reagent ions in the chemical ionization of oxidized multifunctional compounds. *J. Phys. Chem. A* **121**, 269–279 (2018).
62. Wavefunction Inc.: Spartan'14, Irvine, CA (2014).
63. Frisch, M. J. et al. Gaussian 09, Revision D.01; Gaussian, Inc.: Wallingford, CT (2009).
64. Neese, F. The ORCA program system. *Wiley Interdiscip. Rev. Comput. Mol. Sci.* **2**, 73–78 (2012).

Acknowledgements

We thank J. Crounse and T. Kurtén for helpful discussions, K. Pielok and A. Rohmer for technical assistance, and the tofTools team for providing the data analysis toolbox. N.H. thanks the Academy of Finland for funding and CSC–IT Center for Science, Finland, for computational resources.

Author contributions

T.B. designed and conducted the experiments, did the data analysis, and wrote the manuscript. N.H. did the calculations on the stability of the ion-molecule clusters. H.H. contributed to the data interpretation. A.H. supported the development of the mass spectrometric techniques. All authors have discussed and commented on the manuscript.

Additional information

Supplementary information accompanies this paper at https://doi.org/10.1038/s42004-019-0120-9.

Competing interests: The authors declare no competing interests.

Reprints and permission information is available online at http://npg.nature.com/reprintsandpermissions/

Publisher's note: Springer Nature remains neutral with regard to jurisdictional claims in published maps and institutional affiliations.